

Geometric magnetism and anomalous enantio-sensitive observables in photoionization of chiral molecules

Andres F. Ordonez¹, David Ayuso ^{1,2}, Piero Decleva ³ & Olga Smirnova ^{1,4}✉

Chiral molecules are instrumental for molecular recognition in living organisms. Distinguishing between two opposite enantiomers, the mirror twins of the same chiral molecule, is both vital and challenging. Geometric magnetism enables a broad class of phenomena in solids including the anomalous electron velocity, the Hall effect, and related topological observables. Here we show that ultrafast electron currents excited in chiral molecules can generate geometric fields which enable a class of anomalous enantio-sensitive observables in photoionization. Next, we introduce the first member of this class: enantio-sensitive orientation of chiral molecules via photoionization. This effect opens unexplored routes to both enantio-separation and imaging of chiral dynamics on ultrafast time scales. Our work suggests that geometric magnetism in photoionization provides the bridge between the two geometrical properties, chirality and topology.

¹Max-Born-Institut, Berlin, Germany. ²Department of Physics, Imperial College London, London, UK. ³CNR IOM and Dipartimento di Scienze Chimiche e Farmaceutiche, Università degli Studi di Trieste, Trieste, Italy. ⁴Technische Universität Berlin, Berlin, Germany. ✉email: olga.smirnova@mbi-berlin.de

Chiral molecules are characterised by their handedness, an extra degree of freedom of a purely geometrical origin. Geometrical properties in real space are determined by the nuclear configuration in molecules or by the lattice configuration in solids. In solids, they map onto geometrical or topological properties of Hilbert space vectors, leading to robust observables associated with the electronic response to electromagnetic fields and topological phases of matter. Geometric magnetism, introduced by M. Berry¹, is a key concept underlying these phenomena. One of the manifestations of geometric magnetism is the Berry curvature in solids, which enables a class of additional observables in condensed matter systems related to the so-called anomalous electron velocity imparted by the Berry curvature^{2,3}. Can the chiral geometry of molecules lead to similar geometric fields? Here we address this question by considering photoionization of chiral molecules, which can yield very sensitive chiral signals^{4–12}.

We have found a manifestation of Berry curvature emerging due to the interplay between electronic and rotational degrees of freedom in photoionization of chiral molecules and show that it enables an additional class of anomalous, i.e. proportional to the Berry curvature, efficient enantio-sensitive photoionization observables. Crucially, these observables rely on ultrafast excitation of chiral electronic or vibronic currents, linking the concept of geometric magnetism to yet another important concept in ultrafast science: the concept of charge-directed reactivity.

Charge-directed chemical reactivity^{13–20} implies that ultrafast electron dynamics can affect the outcome of chemical reactions, opening an important direction in attochemistry^{14–21}. We show that ultrafast electron currents can lead to opposite orientation of left and right enantiomers of the same molecule upon photoionization of randomly oriented molecules by circularly polarized light, thus presenting an example of enantio-sensitive charge-directed reactivity, with geometric fields and concepts providing a platform for its description. A unified picture of enantio-sensitive effects in photoionization of chiral molecules emerges as a corollary of our approach. It reveals a fundamental connection and complementarity between seemingly disjoint enantio-sensitive phenomena in photoionization by establishing geometric fields as their ubiquitous common origin.

Results and discussion

Geometric field in chiral molecules. Geometric concepts in photoionization of chiral molecules with circularly polarized light originate from the so-called propensity field, which we have introduced recently²². It emerges in photoionization of randomly oriented molecules and involves the vector product of two

conjugated photoionization dipoles ($\mathbf{d}_{\mathbf{k}g}$ in the length or $\mathbf{p}_{\mathbf{k}g}$ in the velocity gauge):

$$\mathbf{B}(\mathbf{k}) = i[\mathbf{d}_{\mathbf{k}g} \times \mathbf{d}_{\mathbf{k}g}^*] = i \frac{[\mathbf{p}_{\mathbf{k}g} \times \mathbf{p}_{\mathbf{k}g}^*]}{(E_k - E_g)^2}, \quad (1)$$

where $E_k = k^2/2$ is the photoelectron energy and E_g is the energy of the initial (e.g. ground) state.

Unexplored physics emerges in photoionization from current carrying states. Consider the superposition of two states $|j\rangle + e^{-i\phi_{ij}}|i\rangle$ ($\phi_{ij} = \omega_{ij}t$, with $\omega_{ij} \equiv \omega_i - \omega_j$ being the transition frequency between the states). In this case, the propensity field acquires an additional term, which encodes the coherence between the excited states:

$$\begin{aligned} \mathbf{B}_{ij}(\mathbf{k}, \phi_{ij}) &= -\frac{1}{2} i [\mathbf{d}_{\mathbf{k}i}^* \times \mathbf{d}_{\mathbf{k}j}] e^{i\phi_{ij}} + \text{c.c.} \\ &\equiv \mathbf{Q}_{ij}(\mathbf{k}) \cos \phi_{ij} + \mathbf{P}_{ij}(\mathbf{k}) \sin \phi_{ij}, \end{aligned} \quad (2)$$

where we have introduced the displacement $\mathbf{Q}_{ij}(\mathbf{k})$ and current $\mathbf{P}_{ij}(\mathbf{k})$ quadratures:

$$\mathbf{Q}_{ij}(\mathbf{k}) \equiv -\Im \left\{ i [\mathbf{d}_{\mathbf{k}i}^* \times \mathbf{d}_{\mathbf{k}j}] \right\}, \quad (3)$$

$$\mathbf{P}_{ij}(\mathbf{k}) \equiv \Re \left\{ i [\mathbf{d}_{\mathbf{k}i}^* \times \mathbf{d}_{\mathbf{k}j}] \right\}. \quad (4)$$

Examples of the displacement $\mathbf{Q}_{ij}(\mathbf{k})$ and current $\mathbf{P}_{ij}(\mathbf{k})$ quadratures for a coherent superposition of $|i\rangle = |\text{LUMO}\rangle$ (lowest unoccupied molecular orbital) and $|j\rangle = |\text{LUMO} + 1\rangle$ in propylene oxide (a chiral molecule) are shown in Fig. 1.

Equation (2) describes the component of the field oscillating at the frequency ω_{ij} . For $i = j = g$, $\phi_{ij} = 0$ and Eq. (2) reduces to Eq. (1). For any number of states, Eqs. (1) and (2) can be generalized as

$$\mathbf{B}(\mathbf{k}, \phi_{ij}) = \frac{1}{2} \sum_{i,j} \left\{ i [\mathbf{d}_{\mathbf{k}j} \times \mathbf{d}_{\mathbf{k}i}^*] \right\} e^{i\phi_{ij}}. \quad (5)$$

Applying inversion ($\mathbf{r} \rightarrow -\mathbf{r}$, $\mathbf{k} \rightarrow -\mathbf{k}$) to reverse molecular handedness, we find that the displacement and current quadratures in left- (S) and right-handed (R) molecules are connected via $\mathbf{Q}_{ij}^{(S)}(\mathbf{k}) = \mathbf{Q}_{ij}^{(R)}(-\mathbf{k})$ and $\mathbf{P}_{ij}^{(S)}(\mathbf{k}) = \mathbf{P}_{ij}^{(R)}(-\mathbf{k})$.

The generalized propensity field Eq. (5) gives rise to three classes of enantio-sensitive observables in photoionization of randomly oriented molecules. For brevity we shall refer to both generalized Eq. (5) and original Eq. (1) fields as the propensity field.

Three classes of enantio-sensitive observables. Enantio-sensitive photoionization observables are defined in the laboratory frame

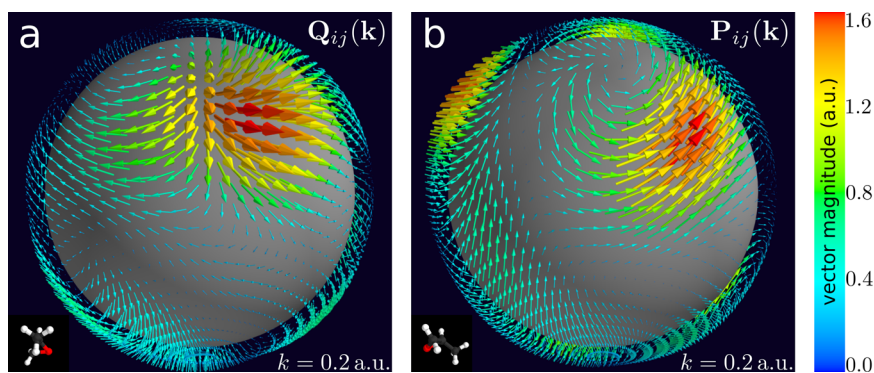


Fig. 1 Quadratures of the propensity field. **a** Displacement $\mathbf{Q}_{ij}(\mathbf{k})$ [Eq. (3)] and **b** current $\mathbf{P}_{ij}(\mathbf{k})$ [Eq. (4)] quadratures of the geometric propensity field $\mathbf{B}_{ij}(\mathbf{k})$ [Eq. (2)] for $|i\rangle = |\text{LUMO}\rangle$ and $|j\rangle = |\text{LUMO} + 1\rangle$ of the chiral molecule propylene oxide and photoelectron momentum $k = 0.2$ a.u. The molecular orientation is shown in the left bottom corner of each panel. Note that the quadratures are shown from different viewpoints. Each point on the grey sphere corresponds to a given direction of \mathbf{k} and each vector to either \mathbf{Q}_{ij} or \mathbf{P}_{ij} for that direction of \mathbf{k} .

and originate from multipoles of the propensity field – quantities surviving averaging over the directions of \mathbf{k} in the molecular frame. We group these multipoles into three categories.

The **first** category includes the *net* propensity field (integrated over all angles ϕ_k, θ_k characterizing the orientation of \mathbf{k} in the molecular frame, $d\Theta_k \equiv d\phi_k d\theta_k \sin \theta_k$):

$$\mathbf{B}_{ij}(k, \phi_{ij}) \equiv \int \mathbf{B}_{ij}(\mathbf{k}, \phi_{ij}) d\Theta_k, \quad (6)$$

The **second** category includes the *net* radial component of the propensity field:

$$[\mathbf{B}_{\parallel}(k, \phi_{ij})]_{ij} \equiv \int \mathbf{B}_{ij}(\mathbf{k}, \phi_{ij}) \cdot \hat{\mathbf{k}} d\Theta_k, \quad \hat{\mathbf{k}} = \frac{\mathbf{k}}{k}. \quad (7)$$

The **third** category includes an infinite array of multipoles ($l \geq 1$) of *net radial* and of the two *net tangential* components of the propensity field:

$$[\mathbf{B}_{\parallel}^{l,m}(k, \phi_{ij})]_{ij} \equiv \int \mathbf{B}_{ij}(\mathbf{k}, \phi_{ij}) \cdot \hat{\mathbf{k}} Y_{lm}(\theta_k, \phi_k) d\Theta_k \quad (8)$$

$$[\mathbf{B}_{\perp,1}^{l,m}(k, \phi_{ij})]_{ij} \equiv \int \mathbf{B}_{ij}(\mathbf{k}, \phi_{ij}) \cdot \nabla_k Y_{lm}(\theta_k, \phi_k) d\Theta_k \quad (9)$$

$$[\mathbf{B}_{\perp,2}^{l,m}(k, \phi_{ij})]_{ij} \equiv \int \mathbf{B}_{ij}(\mathbf{k}) \cdot [\hat{\mathbf{k}} \times \nabla_k] Y_{lm}(\theta_k, \phi_k) d\Theta_k \quad (10)$$

These quantities are the spherical multipole moments of the vector field $\mathbf{B}(\mathbf{k}, \phi_{ij})$ (see e.g.²³).

These three categories lead to three classes of enantio-sensitive observables in photoionization of randomly oriented molecules. Their emergence or cancellation is determined by the time-reversal symmetry of the molecular bound states and the \mathbf{k} -inversion symmetries of the quadratures $\mathbf{Q}_{ij}(\mathbf{k}), \mathbf{P}_{ij}(\mathbf{k})$. It is convenient to introduce symmetric and anti-symmetric superpositions of the quadratures corresponding to left- ($\mathbf{Q}_{ij}^{(S)}, \mathbf{P}_{ij}^{(S)}$) and right-handed ($\mathbf{Q}_{ij}^{(R)}, \mathbf{P}_{ij}^{(R)}$) molecules:

$$\mathbf{Q}_{ij}^{\pm}(\mathbf{k}) = \frac{1}{2} [\mathbf{Q}_{ij}^{(S)}(\mathbf{k}) \pm \mathbf{Q}_{ij}^{(R)}(\mathbf{k})], \quad (11)$$

$$\mathbf{P}_{ij}^{\pm}(\mathbf{k}) = \frac{1}{2} [\mathbf{P}_{ij}^{(S)}(\mathbf{k}) \pm \mathbf{P}_{ij}^{(R)}(\mathbf{k})]. \quad (12)$$

The symmetric superpositions $\mathbf{Q}_{ij}^{+}(\mathbf{k}), \mathbf{P}_{ij}^{+}(\mathbf{k})$ are \mathbf{k} -even and the anti-symmetric superpositions $\mathbf{Q}_{ij}^{-}(\mathbf{k}), \mathbf{P}_{ij}^{-}(\mathbf{k})$ are \mathbf{k} -odd.

The **Class I** of enantio-sensitive observables relies on the existence of the net propensity field Eq. (6). Evidently, the k -odd quadratures $\mathbf{Q}_{ij}^{-}(\mathbf{k})$ and $\mathbf{P}_{ij}^{-}(\mathbf{k})$ do not contribute to this integral. We show (see Methods) that the integral in Eq. (6) vanishes when ionization takes place from a real (time-even) state. Thus, $\mathbf{Q}_{ij}^{+}(\mathbf{k})$ also does not contribute to the net propensity field, which only arises due to the symmetric quadrature $\mathbf{P}_{ij}^{+}(\mathbf{k})$:

$$\begin{aligned} \mathbf{B}_{ij}(k) &= \int \mathbf{B}_{ij}(\mathbf{k}, \phi_{ij}) d\Theta_k = \int \mathbf{P}_{ij}^{+}(\mathbf{k}, \phi_{ij}) d\Theta_k \sin \phi_{ij} \\ &\equiv \mathbf{P}_{ij}^{+}(k) \sin \phi_{ij} \end{aligned} \quad (13)$$

Thus, the enantio-sensitive observables of Class I can only appear if photoionization by a circularly polarized field occurs from current-carrying states ($\sin \phi_{ij} \neq 0$). For example, such states can be generated by a pump pulse, with ionization following ultrafast excitation of a coherent superposition of eigenstates. The fact that the net field $\mathbf{B}_{ij}(k)$ emerges only in systems undergoing dynamics makes it an important player in attosecond photochemistry. In contrast to ring currents excited in atoms or non-chiral molecules by circularly polarized fields^{24–26}, chiral molecules present an example of a system where excited currents do not vanish in the

molecular frame upon averaging over random molecular orientations, because they are protected by the rotationally invariant geometric property of *molecular handedness*. The net propensity field in the molecular frame (13) leads to enantio-sensitive molecular orientation by ionization (see subsection “Anomalous enantio-sensitive observables”) and is an example of charge-directed reactivity emerging solely due to molecular handedness.

The **Class II** of enantio-sensitive observables relies on the existence of the *net radial* component of the propensity field Eq. (7). Clearly, the symmetric quadratures $\mathbf{Q}^{+}(\mathbf{k})$ and $\mathbf{P}^{+}(\mathbf{k})$ do not contribute to $\mathbf{B}_{\parallel}(k)$, leaving us with the following field components allowed by symmetries:

$$[\mathbf{B}_{\parallel}(k, \phi_{ij})]_{ij} = [\mathbf{Q}_{\parallel}^{-}(k)]_{ij} \cos \phi_{ij} + [\mathbf{P}_{\parallel}^{-}(k)]_{ij} \sin \phi_{ij}, \quad (14)$$

$$[\mathbf{Q}_{\parallel}^{-}(k)]_{ij} = \int \mathbf{Q}_{ij}^{-}(\mathbf{k}) \cdot \hat{\mathbf{k}} d\Theta_k, \quad (15)$$

$$[\mathbf{P}_{\parallel}^{-}(k)]_{ij} = \int \mathbf{P}_{ij}^{-}(\mathbf{k}) \cdot \hat{\mathbf{k}} d\Theta_k. \quad (16)$$

The *net radial* component $\mathbf{B}_{\parallel}(k)$ is responsible for the photoelectron circular dichroism (PECD)²⁷, where $[\mathbf{Q}_{\parallel}^{-}(k)]_{ij}$ for $i=j$ leads to PECD for photoionization from a real stationary state. PECD from a superposition of states (time-dependent PECD²⁸) also involves the complementary quadrature $[\mathbf{P}_{\parallel}^{-}(k)]_{ij}$.

The **Class III** of enantio-sensitive observables originates from an infinite array of multipoles ($l \geq 1$) of the *net radial* and of the two *net tangential* components of the propensity field: Eqs. (8)–(10). The parity of spherical harmonics $Y_{lm}(\mathbf{k}) = (-1)^l Y_{lm}(-\mathbf{k})$ dictates that even multipoles $[\mathbf{B}_{\parallel}^{l=2n,m}(k, \phi_{ij})]_{ij}$ and $[\mathbf{B}_{\perp,1}^{l=2n,m}(k, \phi_{ij})]_{ij}$ can only emerge due to the asymmetric quadratures $\mathbf{Q}_{ij}^{-}(\mathbf{k})$ and $\mathbf{P}_{ij}^{-}(\mathbf{k})$, while the odd multipoles $[\mathbf{B}_{\parallel}^{l=2n+1,m}(k, \phi_{ij})]_{ij}$ and $[\mathbf{B}_{\perp,1}^{l=2n+1,m}(k, \phi_{ij})]_{ij}$ can emerge only due to the symmetric quadratures $\mathbf{Q}_{ij}^{+}(\mathbf{k})$ and $\mathbf{P}_{ij}^{+}(\mathbf{k})$. For the $[\mathbf{B}_{\perp,2}^{l,m}(k, \phi_{ij})]_{ij}$ multipoles it is the other way around: the terms with even l may only appear due to the symmetric quadratures $\mathbf{Q}_{ij}^{+}(\mathbf{k})$ and $\mathbf{P}_{ij}^{+}(\mathbf{k})$, while the terms with odd l may emerge only due to $\mathbf{Q}_{ij}^{-}(\mathbf{k})$ and $\mathbf{P}_{ij}^{-}(\mathbf{k})$.

Class III observables emerge in two- or multi-photon ionization of randomly oriented molecules. For example, quadrupolar [$l=1$ in Eq. (8)] PECD currents²⁹ emerge in two-photon ionization of chiral molecules triggered by orthogonally polarized two-color $\omega - 2\omega$ fields. Predicted by Demekhin, Baumert and coworkers^{30,31}, quadrupolar [$l=1$ in Eq. (8)] PECD currents have so far escaped experimental observation. Other members of this class have not been identified so far.

Anomalous enantio-sensitive observables. While the Class II observables have already been detected in experiments, the Class I of anomalous enantio-sensitive observables has not been explored yet. We call these observables anomalous because they are proportional to the Berry curvature (see next section), in analogy to anomalous velocity in solids stemming from the Berry curvature. Class I involves any vectorial observable \mathbf{V} of the cation. Indeed, the orientation-averaged value of a vector \mathbf{V} fixed in the molecular frame, after ionization via circularly polarized light

propagating along the laboratory z axis yields (see Methods)

$$\begin{aligned} \langle \mathbf{V}^L(k) \rangle &\equiv \int W(k, \rho) \mathbf{V}^L(\rho) d\rho \\ &= \frac{1}{2} |\mathcal{E}(\omega)|^2 \sigma \int \left[\int \mathbf{B}^L(\mathbf{k}, \rho) \cdot \hat{\mathbf{z}}^L d\Theta_k \right] \mathbf{V}^L(\rho) d\rho \quad (17) \\ &= \frac{1}{6} |\mathcal{E}(\omega)|^2 \sigma (\mathbf{B}^M(k) \cdot \mathbf{V}^M) \hat{\mathbf{z}}^L. \end{aligned}$$

Here the superscripts L and M indicate vectors expressed in the laboratory and in the molecular frame, respectively, ρ denotes the Euler angles characterizing the orientation of the molecular frame relative to the laboratory frame, $W(k, \rho)$ is the ionization rate for photoelectrons with energy $E_k = k^2/2$ for a fixed in space molecule ionized by circularly polarized light propagating along the laboratory z axis, $\hat{\mathbf{z}}^L$. Equation (17) shows that after ionization, the ensemble-averaged value of any vector \mathbf{V} fixed in the molecular frame will have an *anomalous* (proportional to the net propensity field) enantio-sensitive component along the direction perpendicular to the polarization plane of the ionizing pulse. \mathbf{V} can represent any vector rotating rigidly with the molecule such as a transition or a permanent dipole. Below we focus on the particular molecular axis that (as we will show) becomes oriented upon coherent excitation and subsequent photoionization.

Class I observables require excitation of current prior to photoionization. Consider a pump-probe set-up with two pulses copropagating along the laboratory z axis, $\hat{\mathbf{z}}^L$. The linearly polarized pump pulse excites a coherent superposition of two states with energy difference ω_{12} in a randomly oriented molecular ensemble. The excitation is probed via photoionization by a circularly polarized probe. The net propensity field is $\mathbf{B}_{12}(k, t) = \mathbf{P}_{12}^+(k) \sin(\omega_{12}t)$ and it is fixed in the molecular frame.

Consider a unit polar vector $\hat{\mathbf{e}}_B$ pointing in the direction of the net propensity field $\hat{\mathbf{e}}_B \parallel \mathbf{P}_{12}^+(k)$ in a given enantiomer. $\hat{\mathbf{e}}_B$ and

$\mathbf{P}_{12}^+(k)$ are fixed in the molecular frame (see Fig. 2). The scalar product $\hat{\mathbf{e}}_B \cdot \mathbf{P}_{12}^+(k) = v |\mathbf{P}_{12}^+(k)|$ is a pseudoscalar, which has opposite signs ($v = \pm 1$) in opposite enantiomers. Upon photoionization, the orientation-averaged value of $\hat{\mathbf{e}}_B$ in the laboratory frame is (see Methods)

$$\langle \hat{\mathbf{e}}_B^L(k, \tau) \rangle = R \langle \hat{\mathbf{e}}_B^L(k, \tau) \rangle_{\text{isotropic}}, \quad (18)$$

$$\langle \hat{\mathbf{e}}_B^L(k, \tau) \rangle_{\text{isotropic}} = \frac{1}{9} C \sigma v (\mathbf{d}_{10}^M \cdot \mathbf{d}_{20}^M) |\mathbf{P}_{12}^+(k)| \sin(\omega_{12}\tau) \hat{\mathbf{z}}^L, \quad (19)$$

where R accounts for the molecular alignment induced by the pump,

$$R \equiv \frac{6}{5} \left[1 - \frac{1}{2} \frac{(\mathbf{d}_{10}^M \cdot \hat{\mathbf{e}}_B^M)(\mathbf{d}_{20}^M \cdot \hat{\mathbf{e}}_B^M)}{(\mathbf{d}_{10}^M \cdot \mathbf{d}_{20}^M)} \right], \quad (20)$$

while $\langle \hat{\mathbf{e}}_B^L(k, \tau) \rangle_{\text{isotropic}}$ ignores it; \mathbf{d}_{10} and \mathbf{d}_{20} are the excitation dipoles and C encodes the pump and probe Fourier components at the excitation and photoionization frequencies correspondingly (we consider transform limited pulses):

$$C \equiv |\mathcal{E}_1^*(\omega_{20}) \mathcal{E}_2^*(\omega_{k2}) \mathcal{E}_1(\omega_{10}) \mathcal{E}_2(\omega_{k1})|. \quad (21)$$

Equations (18) and (19) show that the oscillating net propensity field $|\mathbf{P}_{12}^+(k)| \sin(\omega_{12}\tau)$ dictates the orientation of the molecular vector $\hat{\mathbf{e}}_B(k)$ (and thus of the molecule) along the axis perpendicular to the polarization of the circularly polarized probe. The resulting molecular orientation points in opposite directions for either opposite enantiomers ($v = \pm 1$) and a fixed probe polarization σ , or for a fixed enantiomer v and opposite probe polarizations ($\sigma = \pm 1$).

Equations (18) and (19) predict that the enantio-sensitive orientation (the photo-ionization molecular orientation circular dichroism, PI-MOCD) oscillates as a function of the pump-probe delay, reaching maximal positive or negative values for

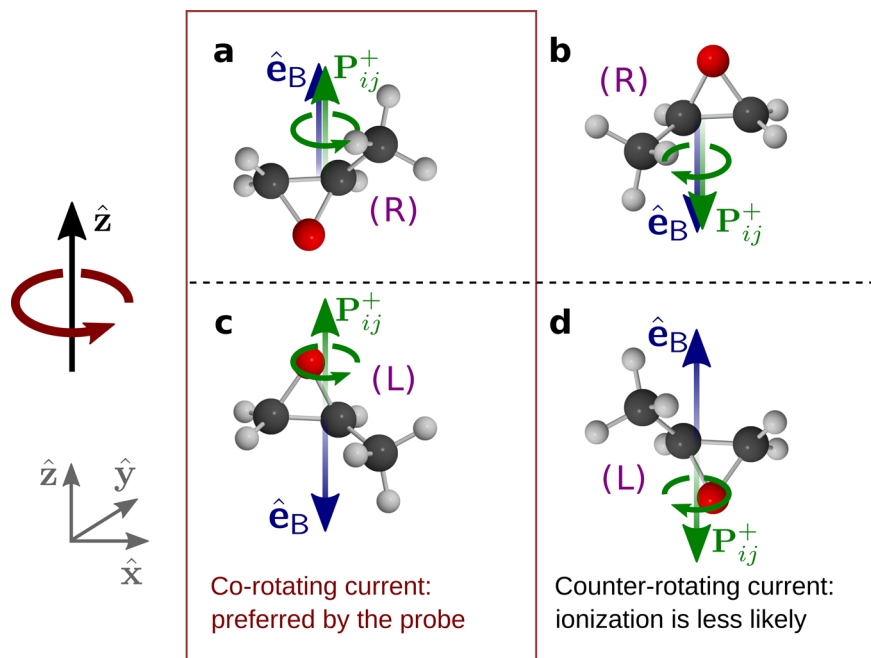


Fig. 2 Enantio-sensitive orientation by photoionization. Relative orientations of the molecular vectors $\hat{\mathbf{e}}_B$ and \mathbf{P}_{ij}^+ for opposite molecular orientations and opposite enantiomers for $k = 0.2$ a.u. and a superposition of $|i\rangle = |\text{LUMO}\rangle$ and $|j\rangle = |\text{LUMO} + 1\rangle$ in propylene oxide. Panels (a) and (b) represent oppositely oriented right enantiomers. Panels (c) and (d) represent oppositely oriented left enantiomers. The red circular arrow shows the rotation direction of the circularly polarized field. The green circular arrows show the circular current in the excited states right before ionization takes place. Photoionization rates are higher for orientations (a) and (c) than for (b) and (d) because ionization is more effective when the electronic current (circular green arrow fixed to \mathbf{P}_{ij}^+) and the electric field rotate in the same direction. This difference in photoionization rates causes enantio-sensitive orientation.

$\tau = (2n - 1)\pi/(2\omega_{12})$, with n a positive integer. Photoionization at opportune times using a circularly polarized probe induces enantio-sensitive orientation of both the molecular cations and of the excited neutrals that were not ionized, with the orientation of the neutrals opposite to that of the cations.

Figure 2 shows the direction of the preferred molecular orientation $\hat{\mathbf{e}}_{\mathbf{B}}$ arising when the excitation of $|1\rangle = |\text{LUMO}\rangle$ and $|2\rangle = |\text{LUMO} + 1\rangle$ in propylene oxide is followed by photoionization into the states with momentum $k = 0.2$ a.u., for the left- and right-handed enantiomers. The quadrature $\mathbf{P}_{12}^+(k)$ has the same direction in the left- and right-handed enantiomers, but the pseudoscalar ν has opposite signs for the opposite enantiomers, corresponding to opposite orientations of left and right molecular ions with respect to the laboratory z axis. To calculate the propensity field, we have used the photo-excitation and photoionization dipoles computed using the density functional theory (DFT)-based approach developed in ref. ³² (see ref. ³³ for computational details). This approach yields excellent agreement with the experimental data for one-photon ionization of chiral molecules^{34–38}.

Figure 3 compares the quadratures responsible for Class I and Class II enantio-sensitive observables for the same excitation. The magnitude of the net quadrature $|\mathbf{P}_{12}^+(k)|$ quantifying the PI-MOCD is substantially larger than each of the quadratures $[\mathbf{Q}_{\parallel}^-(k)]_{12}$ and $[\mathbf{P}_{\parallel}^-(k)]_{12}$ quantifying the time-dependent PECD (TD-PECD):

$$\mathbf{j}_{\text{TD-PECD}}^{\perp}(k, \tau) = \frac{1}{9} \text{Cok}(\mathbf{d}_{10}^{\text{M}} \cdot \mathbf{d}_{20}^{\text{M}}) \times \left\{ \cos(\omega_{12}\tau) [\mathbf{Q}_{\parallel}^-(k)]_{12} + \sin(\omega_{12}\tau) [\mathbf{P}_{\parallel}^-(k)]_{12} \right\} \hat{\mathbf{z}}^{\perp}. \quad (22)$$

In Eq. (22) we have ignored the molecular alignment by the pump and omitted the time-independent contributions to facilitate the comparison with Eq. (19) for PI-MOCD (see Methods).

Figure 3 shows that the enantio-sensitive orientation is at least of the same order of magnitude as the enantio-sensitive signal in TD-PECD²⁸. Importantly, TD-PECD and PI-MOCD involve completely different components of the geometric field and therefore expose different and complementary aspects of chiral dynamics in molecules.

Qualitatively, the orientation induced by photoionization can be understood as follows. First, a linearly polarized pump excites a couple of excited states $|1\rangle$ and $|2\rangle$ and produces a current \mathbf{j}_{12} oscillating at frequency ω_{12} . Suppose that this current goes from the ‘head’ of a molecule to its ‘tail’ in the molecular frame. For two molecules oppositely oriented in the laboratory frame (see Fig. 2a and b), \mathbf{j}_{12} will have the same direction in the molecular frame. This can be shown by noting that \mathbf{j}_{12} depends on the product of the transition amplitudes to states $|1\rangle$ and $|2\rangle$. Second, like a helix, the chiral structure of the molecule converts this linear current into a circular current, which will have the same direction of rotation in the molecular frame for both orientations. Thus, in the laboratory frame, the two oppositely oriented molecules will display circular currents rotating in opposite directions (see circular arrows in Fig. 2a and b). Due to the propensity rules in one-photon ionization, explicitly quantified by the geometric field $\mathbf{B}_{12}(\mathbf{k})$, the circularly polarized probe pulse ‘selects’ (or preferentially ionizes) the orientation with the current co-rotating with the probe pulse. This leads to a difference in the photoionization yields resulting from each orientation and thus to the emergence of oriented molecular ions. Note that for the opposite enantiomer, the chiral structure of the molecules creates the opposite circulating current in the molecular frame, and thus the probe-pulse ‘selects’ the opposite orientation (see Fig. 2c and d).

Importantly, the difference in the angle-integrated ionization yields for the two opposite orientations is proportional to the projection of the net propensity field $\mathbf{B}_{12}(k)$ on the laboratory z axis. Thus, the propensity rule ‘selecting’ molecular orientations with co-rotating current is most pronounced for orientations

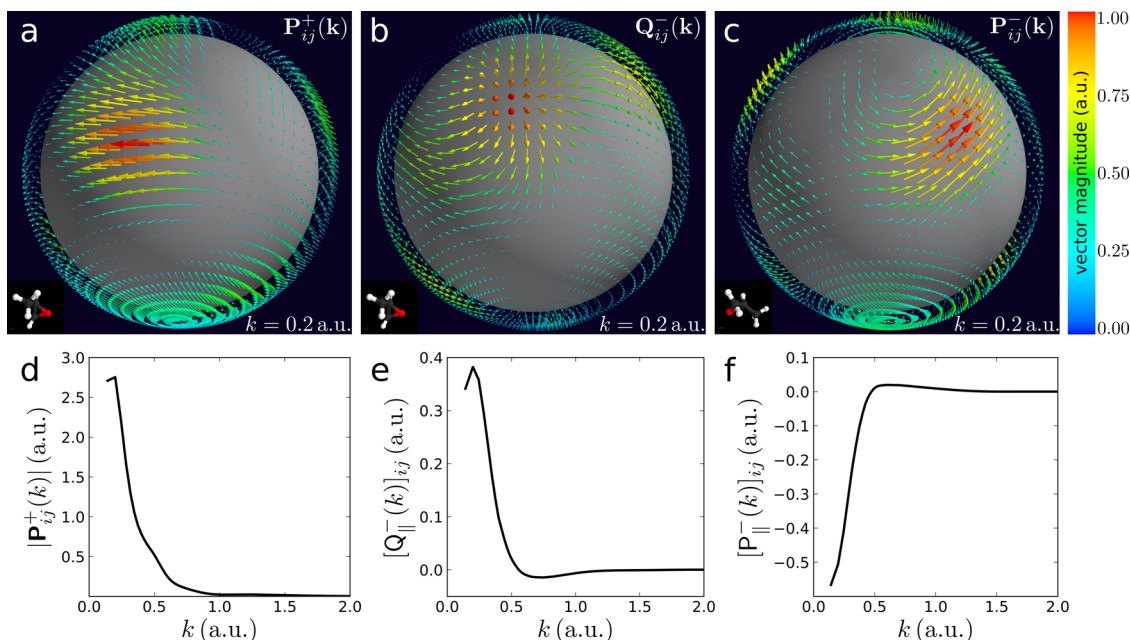


Fig. 3 Geometric propensity field and its multipoles. Net propensity field and the net radial component of the propensity field emerging upon excitation of $|i\rangle = |\text{LUMO}\rangle$ and $|j\rangle = |\text{LUMO} + 1\rangle$ orbitals in propylene oxide. Symmetric $\mathbf{P}_{ij}^+(\mathbf{k})$ [a, Eq. (12)] and asymmetric $\mathbf{Q}_{ij}^-(\mathbf{k})$ [b, Eq. (11)] and $\mathbf{P}_{ij}^-(\mathbf{k})$ [c, Eq. (12)] quadratures for $k = 0.2$ a.u. Each point on the grey sphere corresponds to a given direction of \mathbf{k} and each vector to either \mathbf{P}_{ij}^+ , \mathbf{Q}_{ij}^- , or \mathbf{P}_{ij}^- for that direction of \mathbf{k} . **d** Magnitude of the net value $|\mathbf{P}_{ij}^+(k)|$ [Eq. (13)], which governs Class I observables, such as enantio-sensitive molecular orientation (PI-MOCD) [Eqs. (18), (19)]. **e, f** Net values of the radial components $[\mathbf{Q}_{\parallel}^-(k)]_{ij}$ [d, Eq. (15)] and $[\mathbf{P}_{\parallel}^-(k)]_{ij}$ [f, Eq. (16)], which govern Class II observables, such as the TD-PECD [Eq. (22)].

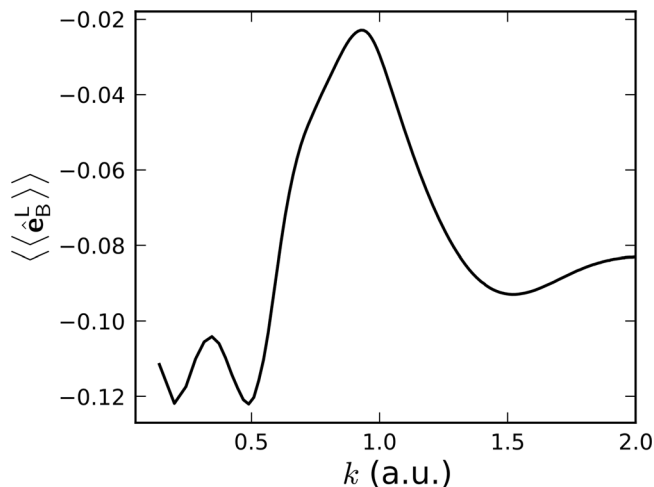


Fig. 4 Molecular orientation circular dichroism. Degree of orientation $\langle\langle \hat{\mathbf{e}}_B^L(k, \tau) \rangle\rangle$ [see Eq. (51) in Methods] obtained after coherent excitation of |LUMO> and |LUMO + 1> in randomly oriented propylene oxide followed by ionization with a circularly polarized pulse, for $\omega_{12}\tau = \pi/2$, $\nu = 1$, and $\sigma = 1$.

where $\mathbf{B}_{12}(k)$ is parallel to the laboratory z axis, which explains why $\mathbf{B}_{12}(k)$ is the molecular axis becoming maximally oriented. The fact that the photoionization yield depends on the direction of the current excited in the chiral molecule prior to photoionization not only explains the emergence of PI-MOCD but is also an example of enantio-sensitive charge-directed reactivity.

Figure 4 shows the degree of orientation of the molecular ions calculated using DFT-based matrix elements, dipole couplings and Eq. (18). The strength of the effect is characterized by the fraction of oriented ions normalized to the averaged over pump-probe delay total ionization rate, $\langle\langle \hat{\mathbf{e}}_B^L(k, \tau) \rangle\rangle$ (see Methods). Having $\langle \cos \theta \rangle = -0.12$ for $k = 0.2$ a.u. means that roughly 59 out of 100 molecules have $\hat{\mathbf{e}}_B^L \cdot \hat{\mathbf{z}}^L < 0$ and 41 out of 100 molecules have $\hat{\mathbf{e}}_B^L \cdot \hat{\mathbf{z}}^L > 0$. Thus, a very significant degree of enantio-sensitive orientation results from the excitation of chiral dynamics in valence shells.

One should not confuse laser-induced orientation via direct excitation of rotational degrees of freedom^{39–42} with the purely electronic effect described here. The initial rotational temperature does indeed play crucial role in the former, but is not relevant in our case of a purely electronic effect which happens on the electronic time-scale. Photoionization-induced orientation of heteronuclear diatomic molecules in a two-color, linearly polarized field⁴³ is another example of electronically induced orientation where the initial rotational temperature is unimportant.

The Berry curvature, Berry connection and Berry phase in photoionization of chiral molecules. The Berry curvature is an example of a geometric field, which emerges as a result of decoupling fast and slow dynamics associated with different degrees of freedom. Decoupling implies that the slow dynamics is included adiabatically; the Berry curvature reflects the presence of non-adiabatic interactions. Below we show that the net propensity field introduced in Eq. (13) is equivalent to the Berry curvature emerging in response to the decoupling of slow molecular rotational and fast electronic motion.

To this end, we can introduce two vastly different time scales t and T , which describe the fast electronic (t) and slow rotational motion (T) correspondingly. In the molecular frame, the electronic response to the light field is coupled to the rotational

degrees of freedom, since the orientation of the molecule defines the direction of the laser field polarization \mathbf{E} in the molecular frame. Thus, the direction of the laser field polarization vector $\mathbf{E}(t, T)$ in the molecular frame depends both on the electronic time t , which describes e.g. the sub-cycle evolution of the laser field, and on the rotational time T , which describes the evolution of molecular orientation in space defined e.g. by a molecular rotational wave-packet. When we solve the time-dependent Schrödinger equation (TDSE) to describe molecular photoionization, which is its electronic response, we can freeze the rotational time, such that the full molecular wave-function $\Psi(t, T)$ depends on T parametrically (see Methods). It means that we neglect the $i\frac{\partial}{\partial T}$ term in the TDSE, when computing the electronic dynamics. As shown by Aharonov and Anandan⁴⁴, the geometric phase accumulated during a cycle T_0 of such adiabatic evolution (T_0 is a rotational period) is given by:

$$\beta = \int_0^{T_0} \langle \psi_I | i \frac{d}{dT} | \psi_I \rangle dT. \quad (23)$$

Thus, we obtain

$$\begin{aligned} \beta &= \int_0^{T_0} i \langle \psi_I(T) | \nabla_{\mathbf{E}} \psi_I(T) \rangle \cdot \frac{d\mathbf{E}(T)}{dT} dT \\ &= \int_{C(\mathbf{E}(T))} i \langle \psi_I(\mathbf{E}) | \nabla_{\mathbf{E}} \psi_I(\mathbf{E}) \rangle \cdot d\mathbf{E} \end{aligned} \quad (24)$$

Here ψ_I is the molecular wave-function in the interaction picture, the cyclic path C parametrized as $C(\mathbf{E}(T))$ is defined by the evolution of the rotational wavepacket. Equation (24) allows us to introduce the Berry connection:

$$\mathbf{A}(\mathbf{E}) = i \langle \psi_I(\mathbf{E}) | \nabla_{\mathbf{E}} \psi_I(\mathbf{E}) \rangle, \quad (25)$$

and the Berry curvature:

$$\Omega = \nabla_{\mathbf{E}} \times \mathbf{A} = i \langle \nabla_{\mathbf{E}} \psi_I(\mathbf{E}) | \times | \nabla_{\mathbf{E}} \psi_I(\mathbf{E}) \rangle. \quad (26)$$

We can now use Eq. (26) to calculate the Berry curvature emerging in photoionization of chiral molecules. Since the Berry curvature is gauge invariant, we can use perturbation theory to calculate $|\psi_I(\mathbf{E})\rangle$ ⁴⁵ explicitly:

$$\psi_I(\mathbf{E}) = \psi_0 + \int d\Theta_k a_k(\mathbf{E}) \psi_k, \quad (27)$$

$$a_k = i \int_0^t dt' \mathbf{d}_{k0} \cdot \mathbf{E}(t') e^{i\omega_k t'} = i \mathbf{d}_{k0} \cdot \mathbf{E}_\omega(\omega_k), \quad (28)$$

$$\nabla_{\mathbf{E}} \psi_I(\mathbf{E}) = \int d\Theta_k i \mathbf{d}_{k0} \psi_k, \quad (29)$$

$$\Omega = \int d\Theta'_k \int d\Theta_k i \langle \psi_{k'} | \psi_k \rangle [\mathbf{d}_{k'0}^* \times \mathbf{d}_{k0}] = i \int d\Theta_k [\mathbf{d}_{k0}^* \times \mathbf{d}_{k0}] \quad (30)$$

Equation (30) is equivalent to the net generalised propensity field [see Eq. (13)].

When transforming the light field to the molecular frame, we can choose the radial direction $\hat{\mathbf{e}}_r$ in this frame to represent the propagation direction of the light in the molecular frame. For randomly oriented molecules, $\hat{\mathbf{e}}_r$ is distributed on a sphere which corresponds to all possible values of angles θ, ϕ defining the direction of light propagation in the molecular frame. The polarization plane of the laser field is tangent to this sphere. For a circularly polarized field we can write $\mathbf{E}(\theta, \phi) = E_\omega^\theta(\theta, \phi) \hat{\mathbf{e}}_\theta + i E_\omega^\phi(\theta, \phi) \hat{\mathbf{e}}_\phi$. As θ and ϕ change, the laser field polarization vector, tangent to the sphere is subject to parallel transport, which is sensitive to the presence or absence of the curvature. Thus, in

the case of randomly oriented molecules, the path $C(\mathbf{E})$ covers the entire sphere.

Using the example of randomly oriented molecules, we can get insight into the physical meaning of the Berry phase in photoionization. To this end, we note that the total, averaged over all random molecular orientations $\rho(\int d\rho = \frac{1}{8\pi^2} \int_0^\pi \sin\theta d\theta \int_0^{2\pi} d\phi \int_0^{2\pi} d\alpha)$, enantio-sensitive photoionization yield

$$\begin{aligned} W^{ES}(k) &= \int W^{ES}(k, \rho) d\rho \\ &= \frac{\sigma}{4\pi} |E_\omega|^2 \int \int \int (\mathbf{B}^L(\mathbf{k}, \rho) \cdot \hat{\mathbf{z}}^L) d\Theta_k \sin\theta d\theta d\phi \\ &= \frac{\sigma}{4\pi} |E_\omega|^2 \int \int \int (\mathbf{B}^M(\mathbf{k}) \cdot \hat{\mathbf{e}}_r^M) d\Theta_k \sin\theta d\theta d\phi \quad (31) \\ &= \frac{\sigma}{4\pi} |E_\omega|^2 \int \int (\boldsymbol{\Omega}^M \cdot \hat{\mathbf{e}}_r^M) \sin\theta d\theta d\phi \\ &= \frac{\sigma}{4\pi} |E_\omega|^2 \int \boldsymbol{\Omega}^M \cdot d\mathbf{S}^M \end{aligned}$$

is equivalent to the flux of the Berry curvature through the surface of a sphere with the area element $d\mathbf{S} = \hat{\mathbf{e}}_r \sin\theta d\theta d\phi$.

The flux in Eq. (31) is equivalent to the sum of two fluxes through the two open surfaces that appear if we cut the sphere equatorially into two hemispheres, the upper S^+ and the lower S^- :

$$\int \boldsymbol{\Omega} \cdot d\mathbf{S} = \int_{S^+} \boldsymbol{\Omega} \cdot d\mathbf{S} + \int_{S^-} \boldsymbol{\Omega} \cdot d\mathbf{S}. \quad (32)$$

Using the Stokes theorem we obtain:

$$\int_{S^\pm} \boldsymbol{\Omega} \cdot d\mathbf{S} = \pm \int_C \mathbf{A}_\pm \cdot d\mathbf{E} = \beta_\pm, \quad (33)$$

where the laser polarization vector \mathbf{E} is tangent to the curve C at every point $\phi = [0, 2\pi]$, $\theta = \pi/2$ and β_\pm is the respective Berry phase for each line integral. Thus, the enantio-sensitive yield is related to the Berry phase:

$$W^{ES}(k) = \frac{\sigma}{4\pi} |E_\omega|^2 \int \boldsymbol{\Omega} \cdot d\mathbf{S} = \frac{\sigma}{4\pi} |E_\omega|^2 (\beta_+ - \beta_-). \quad (34)$$

In the current set-up the enantio-sensitive part of the photoionization yield is zero: $\beta_+ = \beta_-$. To achieve non-zero enantio-sensitive photoionization yield, one may either shape the evolution of the molecular rotational wavepacket or shape the polarization of the laser field, so that the parallel transport of the laser polarization vector occurs along a curve lying on a non-trivial surface. The first strategy may be realised using non-adiabatic molecular alignment prior to ionization^{39–42,46} to create rotational wave-packets with topologically non-trivial surfaces in θ and ϕ , which may lead to quantization of the flux of the Berry curvature piercing these surfaces³. The second opportunity may be realized via application of synthetic chiral light⁴⁷ to photoionization of randomly oriented molecules, because this light leads to enantio-sensitive scalar observables⁴⁸, such as the photoionization yield.

Note that here we have used the concept of cyclic adiabatic evolution to introduce the associated geometric phase. The concept of cyclic evolution is strictly speaking only applicable to spherical tops, because their rotational dynamics is characterized by a single rotational constant leading to a well-defined rotational period. For symmetric tops with two different incommensurate rotational constants, the periodic evolution can be approximated to any desired accuracy within the Dirichlet's approximation theorem. Since the concept of geometric phase has been extended to arbitrary evolutions (non-unitary and non-cyclic)⁴⁹, one should be able to extend the current derivation to this more general case, which will then include asymmetric tops.

Class I observables are proportional to the Berry curvature and as such, they present the first example of anomalous enantio-sensitive observables. The equivalence of the net propensity field and the Berry curvature points to the geometric nature of the propensity field.

Conclusions

We see several future directions associated with geometric fields in photoionization of chiral molecules:

Valence-shell PI-MOCD can be induced by exciting electronic or vibronic degrees of freedom and thus can be achieved with pulses of various durations: from sub-femtoseconds to picoseconds. An interesting future direction is to use PI-MOCD, which occurs both in molecular ions and excited neutral molecules remaining after ionization, for (i) quantification of helical currents in chiral molecules, (ii) enantio-separation and (iii) ultrafast molecular imaging with oriented chiral molecules.

PI-MOCD can also be induced by core excitation with few-femtosecond X-ray pulses. Localised site-specific core excitation could allow one to initiate currents from different locations inside the molecule and probe the orientation of the most efficient molecular corkscrew. Probing the induced electronic excitations should likely be done before the core-hole decay due to e.g. the Auger process. Molecular fragmentation, which may be induced by such decay, could be beneficial for detecting PI-MOCD via angular distributions of fragments.

We have found that PI-MOCD can also be induced using a circularly polarized pump pulse and a linearly polarized probe. In this case, PI-MOCD emerges due to the helical photoexcitation circular dichroism (PXCD) current⁵⁰ excited in bound states and does not involve geometry of photoionization dipoles. PI-MOCD induced by circularly polarized pump and probe pulses records the interference between the PXCD mechanism of PI-MOCD and the geometric mechanism described here. Such interference presents an opportunity to characterize the geometric propensity field experimentally.

Direct experimental detection of the geometric propensity field $\mathbf{B}(\mathbf{k})$ requires measurement of circular dichroism in the photoionization yield for a given photoelectron momentum, resolved on the orientation of molecular frame, for all possible orientations. Experiments⁵¹ indicate that such measurement is within the reach for small-size chiral molecules.

Identification of additional, still hidden members of Classes I, II, and III of enantio-sensitive observables predicted in this work is another exciting direction.

We have shown that Class I enantio-sensitive observables rely on the net propensity field, which is equivalent to the Berry curvature. Since the Berry curvature is at the origin of many topological phenomena, our result provides a way of relating two geometrical properties: chirality and topology. The appearance of the Berry curvature also points to so far undiscovered physics which may emerge due to the coupling of controlled molecular rotations^{39–42} with attosecond electron dynamics. For example, here we have considered enantio-sensitive charge-directed reactivity in randomly rotating molecules. However, one may also consider an initially prepared rotational wavepacket^{39–42} which forms a nontrivial topological structure during its temporal evolution. This structure, probed by photo-ionization as a function of the delay between the pulses exciting the rotational and electronic dynamics, may manifest itself in quantized enantio-sensitive photoionization yield.

Overall, merging chiral and topological ultrafast effects in chiral molecular gases in electric-dipole approximation may lead to breakthrough applications in enantio-sensitive imaging and control of chiral molecules.

Class I enantio-sensitive phenomena require violation of time-reversal symmetry, which can be achieved due to excitation of electron dynamics, considered here, or due to spin-orbit interaction. Spin-resolved photoionization of chiral molecules was pioneered by Cherepkov⁵. Uncovering the role of the Berry curvature in it is another important direction.

In the context of spin-resolved processes, our results establishing the connection between the Berry curvature and the Class I of enantio-sensitive observables, may have a broader scope in the context of experiments on angular-resolved fragmentation of nuclei⁵².

As an entrant to the family of geometric fields, the Berry curvature in chiral molecules, described here, provides an path to exploring the interplay between chiral and topological phenomena in chiral molecules and solids. Our work, together with the recent work⁵³ exploring a topological frequency conversion in chiral molecules induced by the microwave fields, provide the first steps along this path.

Methods

Operator approach and time-reversal symmetry of the net geometric propensity field. Here we prove that

$$\int d\Theta_k \mathbf{Q}_{ij}(\mathbf{k}) = 0 \quad (35)$$

when $|\psi_i\rangle$ and $|\psi_j\rangle$ are time-even states, which we use in Eq. (13).

The time-reversal symmetry plays a central role in enabling the net geometric propensity field. To consider the parity of the geometric propensity field (or its quadratures) with respect to time-reversal, it is convenient⁵⁴ to introduce an operator approach. Equation (2) of the main text can be rewritten in the following form:

$$\mathbf{B}_{ij}(\mathbf{k}, \phi_{ij}) = -\frac{1}{2}i \left[\mathbf{d}_{ki}^* \times \mathbf{d}_{kj} \right] e^{i\phi_{ij}} + \text{c.c.} = -\frac{1}{2}\mathbf{F}_{ij} e^{i\phi_{ij}} + \text{c.c.}, \quad (36)$$

where $\mathbf{F}_{ij}(\mathbf{k}) \equiv i \left[\mathbf{d}_{ki}^* \times \mathbf{d}_{kj} \right]$ and thus,

$$\mathbf{Q}_{ij}(\mathbf{k}) \equiv -\Re \left\{ \mathbf{F}_{ij}(\mathbf{k}) \right\}, \quad (37)$$

$$\mathbf{P}_{ij}(\mathbf{k}) \equiv \Im \left\{ \mathbf{F}_{ij}(\mathbf{k}) \right\}. \quad (38)$$

To establish the parity of net quadratures with respect to time-reversal, it is sufficient to consider the time-reversal parity of the net $\mathbf{F}_{ij}(\mathbf{k})$:

$$\mathbf{F}_{ij} \equiv \int d\Theta_k i \mathbf{d}_{ki}^* \times \mathbf{d}_{kj}. \quad (39)$$

Analogously to the procedure in ref. 54, we rewrite \mathbf{F}_{ij} as the matrix element of an operator $\hat{\mathbf{F}}$:

$$\begin{aligned} \mathbf{F}_{ij} &\equiv \int d\Theta_k i \mathbf{d}_{ki}^* \times \mathbf{d}_{kj} = \int d\Theta_k i \langle \psi_i | \hat{\mathbf{r}} | \psi_k^{(-)} \rangle \\ &\times \langle \psi_k^{(-)} | \hat{\mathbf{r}} | \psi_j \rangle = \langle \psi_i | \hat{\mathbf{F}} | \psi_j \rangle, \end{aligned} \quad (40)$$

where the operator $\hat{\mathbf{F}}$ in vector and component form is given by

$$\begin{aligned} \hat{\mathbf{F}} &\equiv i \int d\Theta_k \hat{\mathbf{r}} | \psi_k^{(-)} \rangle \langle \psi_k^{(-)} | \hat{\mathbf{r}}; \quad \hat{F}_a = i \epsilon_{abc} \int d\Theta_k \hat{r}_b \hat{P}_k \hat{r}_c \\ &= i \epsilon_{abc} \hat{r}_b \hat{P}_k \hat{r}_c, \end{aligned} \quad (41)$$

and $\hat{P}_k \equiv \int d\Theta_k | \psi_k^{(-)} \rangle \langle \psi_k^{(-)} |$ is the projector on the subspace of all states with energy $E = k^2/2$. Since $\hat{\mathbf{r}}$ and \hat{P}_k are Hermitian, $\hat{\mathbf{F}}$ is

also Hermitian:

$$\hat{F}_a^\dagger = (i \epsilon_{abc} \hat{r}_b \hat{P}_k \hat{r}_c)^\dagger = -i \epsilon_{abc} \hat{r}_c \hat{P}_k \hat{r}_b = i \epsilon_{acb} \hat{r}_c \hat{P}_k \hat{r}_b = \hat{F}_a. \quad (42)$$

Now we want to see how time reversal considerations constraint the matrix elements of $\hat{\mathbf{F}}$. Let \hat{T} be the time-reversal operator (see e.g. sec. 4.4 in ref. 55). \hat{T} converts a state $|\alpha\rangle$ into its time-reversed counterpart $|\tilde{\alpha}\rangle = \hat{T}|\alpha\rangle$, which we denote by a tilde. \hat{T} is anti-unitary, i.e. $\langle \tilde{\alpha} | \tilde{\beta} \rangle = \langle \alpha | \beta \rangle^*$ and $T(c_1|\alpha\rangle + c_2|\beta\rangle) = c_1^*|\tilde{\alpha}\rangle + c_2^*|\tilde{\beta}\rangle$. A Hermitian operator \hat{A} is time-even (+) or time-odd (-) when $\hat{T}\hat{A} = \pm \hat{A}\hat{T}$. Time parity restricts the matrix elements of \hat{A} according to $\langle \alpha | \hat{A} | \beta \rangle = \pm \langle \tilde{\alpha} | \hat{A} | \tilde{\beta} \rangle^*$. In particular, if \hat{A} is time-odd and the states are time-even (i.e. $|\tilde{\alpha}\rangle = |\alpha\rangle$ and $|\tilde{\beta}\rangle = |\beta\rangle$), it follows that $\langle \alpha | \hat{A} | \beta \rangle = -\langle \alpha | \hat{A} | \beta \rangle^*$ and thus $\Re\{\langle \alpha | \hat{A} | \beta \rangle\} = 0$.

For \hat{P}_k we have

$$\begin{aligned} \hat{T}\hat{P}_k|\phi\rangle &= \hat{T} \left[\int d\Theta_k | \psi_k^{(-)} \rangle \langle \psi_k^{(-)} | \phi \rangle \right] = \int d\Theta_k | \tilde{\psi}_k^{(-)} \rangle \langle \psi_k^{(-)} | \phi \rangle^* \\ &= \int d\Theta_k | \tilde{\psi}_k^{(-)} \rangle \langle \tilde{\psi}_k^{(-)} | \tilde{\phi} \rangle = \hat{P}_k \hat{T} | \phi \rangle \end{aligned} \quad (43)$$

where $\hat{P}_k \equiv \int d\Theta_k | \tilde{\psi}_k^{(-)} \rangle \langle \tilde{\psi}_k^{(-)} |$ also projects on the subspace of all states with energy $E = k^2/2$. Since \hat{P}_k and \hat{P}_k project on the same subspace we must have $\hat{P}_k = \hat{P}_k$ and thus \hat{P}_k is time-even. Furthermore, since $\hat{\mathbf{r}}$ is also time-even, we can use the anti-unitary character of \hat{T} to find that

$$\hat{T}\hat{F}_a|\phi\rangle = \hat{T}(i \epsilon_{abc} \hat{r}_b \hat{P}_k \hat{r}_c |\phi\rangle) = -i \epsilon_{abc} \hat{r}_b \hat{P}_k \hat{r}_c \hat{T}|\phi\rangle = -\hat{F}_a \hat{T}|\phi\rangle, \quad (44)$$

which means that $\hat{\mathbf{F}}$ is time-odd. Thus, $\Re\{\mathbf{F}_{ij}\} = 0$ when $|\psi_i\rangle$ and $|\psi_j\rangle$ are time-even states. Finally, using Eqs. (37) and (38) we obtain for time-even states $|\psi_i\rangle$ and $|\psi_j\rangle$:

$$\int d\Theta_k \mathbf{Q}_{ij}(\mathbf{k}) = - \int d\Theta_k \Re \left\{ \mathbf{F}_{ij}(\mathbf{k}) \right\} = -\Re \left\{ \mathbf{F}_{ij} \right\} = 0, \quad (45)$$

Furthermore, the time-odd parity of $\hat{\mathbf{F}}$ does not restrict the value of net momentum quadrature, which in general is non-zero:

$$\int d\Theta_k \mathbf{P}_{ij}(\mathbf{k}) = \int d\Theta_k \Im \left\{ \mathbf{F}_{ij}(\mathbf{k}) \right\} = \Im \left\{ \mathbf{F}_{ij} \right\} \neq 0. \quad (46)$$

The origin of Class I enantio-sensitive observables. The connection between enantio-sensitive observables in photoionization and the geometric field becomes evident as soon as we consider the photoionization rate $W(k)$ into energy $E = k^2/2$ for a fixed in space molecule ionized by circularly polarized light in the electric-dipole approximation^{5,56}:

$$W(k, \rho) \propto \int d\Theta_k |a_{kc}|^2 \quad (47)$$

$$|a_{kc}|^2 = \frac{1}{2} |\mathcal{E}(\omega)|^2 \left\{ |\mathbf{d}_{kc}^L(\rho) \cdot \hat{\mathbf{x}}^L|^2 + |\mathbf{d}_{kc}^L(\rho) \cdot \hat{\mathbf{y}}^L|^2 + \sigma \mathbf{B}^L(\mathbf{k}, \rho) \cdot \hat{\mathbf{z}}^L \right\}. \quad (48)$$

Here a_{kc} is the amplitude of ionization from a complex-valued randomly oriented bound state $|\psi_c\rangle$ (at this point we do not specify how this state was created in a randomly oriented molecular ensemble and assume that it is given to us) into the final state with photoelectron momentum \mathbf{k} , $\mathcal{E}(\omega)$ is the Fourier (we define the Fourier transform as $\hat{\mathbf{E}}(\omega) = \int_{-\infty}^{\infty} \mathbf{E}(t) e^{i\omega t} dt$ and assume $\hat{\mathbf{E}}(\omega) = \mathcal{E}(\omega)(\hat{\mathbf{x}} - i\sigma\hat{\mathbf{y}})/\sqrt{2}$ at the transition frequency)

component of the light field at the transition frequency ω , $\sigma = \pm 1$ for light rotating clockwise/counterclockwise in the xy plane, integration over $d\Theta_k$ describes averaging over the directions of the photoelectron momentum, ρ denotes the Euler angles characterizing the orientation of the molecular frame relative to the laboratory frame, the vectors \hat{x}^L , \hat{y}^L , and \hat{z}^L denote the axes of the laboratory frame, $\mathbf{d}_{\text{kc}}^L(\rho)$ is the photoionization dipole in the laboratory frame (denoted by superscript L), and $\mathbf{B}^L(\mathbf{k}, \rho)$ is the geometric propensity field in the laboratory frame.

Using Eq. (48) we formally obtain the expression for the orientation-averaged value of an arbitrary vectorial observable $\mathbf{V}^L(k)$ of the molecular cation:

$$\begin{aligned} \langle \mathbf{V}^L(k) \rangle &\equiv \int d\rho W(k, \rho) \mathbf{V}^L(\rho) \\ &= \frac{1}{2} |\mathcal{E}(\omega)|^2 \sigma \int \left[\int \mathbf{B}^L(\mathbf{k}, \rho) \cdot \hat{z}^L d\Theta_k \right] \mathbf{V}^L(\rho) d\rho \quad (49) \\ &= \frac{1}{6} |\mathcal{E}(\omega)|^2 \sigma (\mathbf{B}^M(k) \cdot \mathbf{V}^M) \hat{z}^L. \end{aligned}$$

Here the superscripts L and M indicate that the respective vectors are expressed with respect to the laboratory frame or the molecular frame, correspondingly. Equation (49) shows that after ionization with circularly polarized light, the ensemble-averaged value of the vector \mathbf{V} (fixed in the molecular frame), will have an *anomalous*, i.e. proportional to the Berry curvature (which in chiral molecules is equivalent to net propensity field), enantio-sensitive component along the direction perpendicular to the polarization plane.

Equations describing the MOCD. Suppose that $\hat{\mathbf{e}}_B$ is a unit polar vector collinear with the net geometric propensity field $\hat{\mathbf{e}}_B \parallel \mathbf{B}(k)$ in a given enantiomer. Both $\hat{\mathbf{e}}_B$ and $\mathbf{B}(k)$ are fixed in the molecular frame. The scalar product $\hat{\mathbf{e}}_B \cdot \mathbf{B}(k) = v|\mathbf{B}(k)|$ is a pseudoscalar ($v = \pm 1$), which has opposite signs in opposite enantiomers. The orientation-averaged value of the vector $\hat{\mathbf{e}}_B$ in the laboratory frame is given by [see Eq. (49)]:

$$\langle \hat{\mathbf{e}}_B^L(k) \rangle = \frac{1}{6} |\mathcal{E}(\omega)|^2 \sigma v |\mathbf{B}^M(k)| \hat{z}^L. \quad (50)$$

Therefore, Eqs. (49) and (50) predict enantio-sensitive orientation of molecular ions by ionization. The vector $\hat{\mathbf{e}}_B(k)$ gets oriented along the laboratory z axis (perpendicular to the polarization of the circularly polarized probe).

Now we can specify the procedure of exciting the state $|\psi_c\rangle$ in a randomly oriented molecular ensemble. The complex-valued state $|\psi_c\rangle$ corresponds to excitation of a complex superposition of states prior to photoionization, which can be excited with a linearly polarized pump pulse.

Using our approach^{56,57} we can calculate the orientation of the vector $\hat{\mathbf{e}}_B$ in a molecular cation analytically for the excitation of two intermediate states with energy difference $\omega_{2,1}$ in an ensemble of randomly oriented chiral molecules. Equations (18) and (19) of the main text can be obtained using Eqs. (30)-(35) in ref. 56 and replacing \mathbf{k} by $\hat{\mathbf{e}}_B$, choosing a pump linearly polarized along either the x or y laboratory axes, and a probe circularly polarized in the xy plane (both pulses are transform limited). To express all resulting terms via the vector product of two ionization dipoles, we used the Binet-Cauchy identity $(\mathbf{A} \times \mathbf{B}) \cdot (\mathbf{C} \times \mathbf{D}) = (\mathbf{A} \cdot \mathbf{C})(\mathbf{B} \cdot \mathbf{D}) - (\mathbf{A} \cdot \mathbf{D})(\mathbf{B} \cdot \mathbf{C})$ and the vector triple product identity $\mathbf{A} \times (\mathbf{B} \times \mathbf{C}) = (\mathbf{A} \cdot \mathbf{C})\mathbf{B} - (\mathbf{A} \cdot \mathbf{B})\mathbf{C}$.

The strength of the effect is characterized by the fraction of oriented ions normalized to the total ionization yield (averaged

over pump-probe delay).

$$\langle \langle \hat{\mathbf{e}}_B^L(k, \tau) \rangle \rangle \equiv \frac{\int d\rho \hat{\mathbf{e}}_B^L(\rho) W(k, \rho)}{\int d\rho \overline{W}(k, \rho)}, \quad (51)$$

$$\int d\rho \overline{W}(k, \rho) = \sum_{i=1,2} \frac{|C_i|^2}{30} \int d\Theta_k \left[3|\mathbf{d}_{i0}|^2 |\mathbf{d}_{ki}|^2 - |\mathbf{d}_{i0} \cdot \mathbf{d}_{ki}|^2 \right], \quad (52)$$

and $C_i \equiv -\mathcal{E}(\omega_{i0})\mathcal{E}(\omega_{ki})$. These equations are used to calculate the results shown in Fig. 4. Assuming that intensity of the two spectral components is the same in each pulse, $|\mathcal{E}_i(\omega_{1,0})| = |\mathcal{E}_i(\omega_{2,0})|$ for $i=1,2$, the information about pulse intensities drops out from the results: $|C_1|^2 = |C_2|^2 = |C|^2$, where $|C|$ is given by Eq. (21).

An estimate of the number of ‘up’ N_+ and ‘down’ N_- molecules for $\langle \cos \theta \rangle = -0.12$ can be performed using a simple model for the angular distribution of oriented molecules: $\Psi(\theta) = a_0 Y_{00}(\theta) + a_1 Y_{10}(\theta)$, where $a_0^2 + a_1^2 = 1$. Then $\langle \cos \theta \rangle = \int_0^\pi d\theta \int_0^{2\pi} d\Phi \sin \theta \cos \theta |\Psi(\theta)|^2$, and we can obtain $N_+ \equiv \int_0^{\pi/2} d\theta \int_0^{2\pi} d\phi \sin \theta |\Psi(\theta)|^2 = \frac{1}{4}(2 + 3\langle \cos \theta \rangle) = 0.41$ and $N_- \equiv \int_{\pi/2}^\pi d\theta \int_0^{2\pi} d\phi \sin \theta |\Psi(\theta)|^2 = 1 - N_+ = 0.59$.

Method of multiple scales. To derive the adiabatic decoupling of rotational and electronic degrees of freedom, we write the Hamiltonian as a sum of its rotational \hat{H}_r and field-free electronic \hat{H}_{el} parts, with the operator $\mathbf{r} \cdot \mathbf{E}_L(\rho, t)$ describing the coupling of the ionizing light field and the molecule:

$$i \frac{\partial}{\partial t} \psi(\mathbf{r}, \rho, t) = (H_{el} + H_{rot} + \mathbf{r} \cdot \mathbf{E}_L(\rho, t)) \psi(\mathbf{r}, \rho, t) \quad (53)$$

Here ρ describes the Euler angles characterizing the direction of the laser field in the molecular frame. The standard adiabatic approximation implies that the full wave-function can be represented as a product of its electronic and rotational components:

$$\psi(\mathbf{r}, \rho, t) = \psi_{el}(\mathbf{r}, \rho, t) \psi_{rot}(\rho, t). \quad (54)$$

Substituting Eq. (54) in Eq. (53) and assuming that rotational dynamics is not affected by photoionization, we obtain the following equations for the two components:

$$i \frac{\partial}{\partial t} \psi_{rot}(\rho, t) = H_{rot} \psi_{rot}(\rho, t) \quad (55)$$

$$\langle \psi_{rot}(\rho, t) | i \frac{\partial}{\partial t} \psi_{el}(\mathbf{r}, \rho, t) | \psi_{rot}(\rho, t) \rangle \quad (56)$$

$$= \langle \psi_{rot}(\rho, t) | (H_{el} + \mathbf{r} \cdot \mathbf{E}_L(\rho, t)) \psi_{el}(\mathbf{r}, \rho, t) | \psi_{rot}(\rho, t) \rangle.$$

Assuming narrow rotational wave-packets, Eq. (56) can be further simplified by expanding electronic wave-function $\psi_{el}(\mathbf{r}, \rho, t)$ and the light field $\mathbf{E}_L(\rho, t)$ around a center of rotational wave-packet $\bar{\rho}(t) = \langle \psi_{rot}(\rho, t) | \rho | \psi_{rot}(\rho, t) \rangle$ in Taylor series up to the terms of the first order: $\psi_{el}(\mathbf{r}, \rho, t) = \psi_{el}(\mathbf{r}, \bar{\rho}(t), t) + (\rho - \bar{\rho}(t)) \frac{\partial}{\partial \bar{\rho}(t)} \psi_{el}(\mathbf{r}, \bar{\rho}(t), t)$, $E_L^j(\rho, t) = E_L^j(\bar{\rho}(t), t) + (\rho - \bar{\rho}(t)) \frac{\partial}{\partial \bar{\rho}(t)} E_L^j(\bar{\rho}(t), t)$, $\frac{\partial}{\partial t} \psi_{el}(\mathbf{r}, \rho, t) = \frac{\partial}{\partial t} \psi_{el}(\mathbf{r}, \bar{\rho}(t), t) + \frac{\partial}{\partial \bar{\rho}(t)} \psi_{el}(\mathbf{r}, \bar{\rho}(t), t) \frac{\partial \bar{\rho}(t)}{\partial t} + \frac{\partial}{\partial t} \left[(\rho - \bar{\rho}(t)) \frac{\partial}{\partial \bar{\rho}(t)} \psi_{el}(\mathbf{r}, \bar{\rho}(t), t) \right]$, we can now rewrite Eq. (56) as:

$$\begin{aligned} i \frac{\partial}{\partial t} \psi_{el}(\mathbf{r}, \bar{\rho}(t), t) + \frac{\partial \bar{\rho}(t)}{\partial t} \frac{\partial}{\partial \bar{\rho}(t)} \psi_{el}(\mathbf{r}, \bar{\rho}(t), t) \\ = (H_{el} + \mathbf{r} \cdot \mathbf{E}_L(\bar{\rho}(t), t)) \psi_{el}(\mathbf{r}, \bar{\rho}(t), t). \end{aligned} \quad (57)$$

Equation (57) contains two different time scales: rotational and electronic. The rotational time scale enters via the evolution of the average orientation $\bar{\rho}(t)$. Using the method of multiple scales⁵⁸, we introduce rotational time T in the argument of the average

orientation angle $\bar{\rho}(T)$:

$$i \frac{\partial}{\partial t} \psi_{el}(\mathbf{r}, \bar{\rho}(T), t) + i \frac{\partial}{\partial T} \psi_{el}(\mathbf{r}, \bar{\rho}(T), t) = (H_{el} + \mathbf{r} \cdot \mathbf{E}_L(\bar{\rho}(T), t)) \psi_{el}(\mathbf{r}, \bar{\rho}(T), t). \quad (58)$$

The adiabatic approximation implies that we neglect $\frac{\partial \psi_{el}}{\partial T}$, i.e. we keep T fixed while evaluating photoionization. Thus, after a cycle of adiabatic evolution, the electronic wave-function acquires the Berry phase:

$$\beta = \int_0^{T_0} \left\langle \psi_{el} \left| i \frac{d}{dT} \right| \psi_{el} \right\rangle dT. \quad (59)$$

leading to Eq. (23) of the main text.

Data availability

The data that support the plots within this paper and other findings of this study are available from the corresponding authors upon reasonable request.

Received: 17 July 2023; Accepted: 21 August 2023;

Published online: 18 September 2023

References

- Berry, M. V. Quantal phase factors accompanying adiabatic changes. *Proc. Royal Society of London. A. Mathematical and Phys. Sci.* **392**, 45–57 (1984).
- Resta, R. Macroscopic polarization in crystalline dielectrics: the geometric phase approach. *Rev. Mod. Phys.* **66**, 899–915 (1994).
- Xiao, D., Chang, M.-C. & Niu, Q. Berry phase effects on electronic properties. *Rev. Mod. Phys.* **82**, 1959–2007 (2010).
- Ritchie, B. Theory of the angular distribution of photoelectrons ejected from optically active molecules and molecular negative ions. *Phys. Rev. A* **13**, 1411–1415 (1976).
- Cherepkov, N. Manifestations of the optical activity of molecules in the dipole photoeffect. *J. Phys. B: Atomic Mol. Phys.* **16**, 1543 (1983).
- Powis, I. Photoelectron circular dichroism of the randomly oriented chiral molecules glyceraldehyde and lactic acid. *J. Chem. Phys.* **112**, 301–310 (2000).
- Böwering, N. et al. Asymmetry in photoelectron emission from chiral molecules induced by circularly polarized light. *Phys. Rev. Lett.* **86**, 1187–1190 (2001).
- Nahon, L., Garcia, G. A. & Powis, I. Valence shell one-photon photoelectron circular dichroism in chiral systems. *J. Electron Spectroscopy Related Phenomena* **204**, 322–334 (2015).
- Janssen, M. H. M. & Powis, I. Detecting chirality in molecules by imaging photoelectron circular dichroism. *Phys. Chem. Chem. Phys.* **16**, 856–871 (2014).
- Lux, C. et al. Circular dichroism in the photoelectron angular distributions of camphor and fenchone from multiphoton ionization with femtosecond laser pulses. *Angewandte Chemie International Edition* **51**, 5001–5005 (2012).
- Lehmann, C. S., Ram, N. B., Powis, I. & Janssen, M. H. M. Imaging photoelectron circular dichroism of chiral molecules by femtosecond multiphoton coincidence detection. *J. Chem. Phys.* **139**, 234307 (2013).
- Beaulieu, S. et al. Universality of photoelectron circular dichroism in the photoionization of chiral molecules. *New J. Phys.* **18**, 102002 (2016).
- Weinkauff, R., Schlag, E., Martinez, T. & Levine, R. Nonstationary electronic states and site-selective reactivity. *J. Phys. Chem. A* **101**, 7702–7710 (1997).
- Cederbaum, L. & Zobeley, J. Ultrafast charge migration by electron correlation. *Chem. Phys. Lett.* **307**, 205–210 (1999).
- Breidbach, J. & Cederbaum, L. S. Migration of holes: Formalism, mechanisms, and illustrative applications. *J. Chem. Phys.* **118**, 3983–3996 (2003).
- Remacle, F. & Levine, R. D. An electronic time scale in chemistry. *Proc. Natl. Acad. Sci.* **103**, 6793–6798 (2006).
- Kuleff, A. I. & Cederbaum, L. S. Ultrafast correlation-driven electron dynamics. *J. Phys. B: Atomic, Mol. Optic. Phys.* **47**, 124002 (2014).
- Calegari, F. et al. Ultrafast electron dynamics in phenylalanine initiated by attosecond pulses. *Science* **346**, 336–339 (2014).
- Nisoli, M., Decleva, P., Calegari, F., Palacios, A. & Martín, F. Attosecond electron dynamics in molecules. *Chem. Rev.* **117**, 10760–10825 (2017). PMID: 28488433.
- Delgado, J. et al. Molecular fragmentation as a way to reveal early electron dynamics induced by attosecond pulses. *Faraday Discuss.* **228**, 349–377 (2021).
- Corkum, P. B., Ivanov, M. Y. & Wright, J. S. Subfemtosecond processes in strong laser fields. *Ann. Rev. Phys. Chem.* **48**, 387–406 (1997).
- Ordóñez, A. F. & Smirnova, O. Propensity rules in photoelectron circular dichroism in chiral molecules. I. Chiral hydrogen. *Phys. Rev. A* **99**, 043416 (2019).
- Barrera, R. G., Estevez, G. A. & Giraldo, J. Vector spherical harmonics and their application to magnetostatics. *Eur. J. Phys.* **6**, 287 (1985).
- Eckart, S. et al. Ultrafast preparation and detection of ring currents in single atoms. *Nat. Phys.* **14**, 701–704 (2018).
- Barth, I. & Manz, J. Electric ring currents in atomic orbitals and magnetic fields induced by short intense circularly polarized π laser pulses. *Phys. Rev. A* **75**, 012510 (2007).
- Guo, J., Yuan, K.-J., Lu, H. & Bandrauk, A. D. Spatiotemporal evolution of ultrafast magnetic-field generation in molecules with intense bichromatic circularly polarized uv laser pulses. *Phys. Rev. A* **99**, 053416 (2019).
- Ordóñez, A. F. & Smirnova, O. Propensity rules in photoelectron circular dichroism in chiral molecules. II. General picture. *Phys. Rev. A* **99**, 043417 (2019).
- Comby, A. et al. Relaxation dynamics in photoexcited chiral molecules studied by time-resolved photoelectron circular dichroism: Toward chiral femtochemistry. *J. Phys. Chem. Lett.* **7**, 4514–4519 (2016).
- Ordóñez, A. F. & Smirnova, O. Disentangling enantiosensitivity from dichroism using bichromatic fields. *Phys. Chem. Chem. Phys.* **24**, 7264–7273 (2022).
- Demekhin, P. V., Artemyev, A. N., Kastner, A. & Baumert, T. Photoelectron circular dichroism with two overlapping laser pulses of carrier frequencies ω and 2ω linearly polarized in two mutually orthogonal directions. *Phys. Rev. Lett.* **121**, 253201 (2018).
- Demekhin, P. V. Photoelectron circular dichroism with Lissajous-type bichromatic fields: One-photon versus two-photon ionization of chiral molecules. *Phys. Rev. A* **99**, 063406 (2019).
- Toffoli, D., Stener, M., Fronzoni, G. & Decleva, P. Convergence of the multicenter b-spline dft approach for the continuum. *Chemical Phys.* **276**, 25–43 (2002).
- Ayuso, D., Decleva, P., Patchkovskii, S. & Smirnova, O. Chiral dichroism in bi-elliptical high-order harmonic generation. *J. Phys. B: Atomic, Mol. Optical Phys.* **51**, 06LT01 (2018).
- Turchini, S. et al. Circular dichroism in photoelectron spectroscopy of free chiral molecules: Experiment and theory on methyl-oxirane. *Phys. Rev. A* **70**, 014502 (2004).
- Stener, M., Fronzoni, G., Tommaso, D. D. & Decleva, P. Density functional study on the circular dichroism of photoelectron angular distribution from chiral derivatives of oxirane. *J. Chem. Phys.* **120**, 3284–3296 (2004).
- Stranges, S. et al. Valence photoionization dynamics in circular dichroism of chiral free molecules: The methyl-oxirane. *J. Chem. Phys.* **122**, 244303 (2005).
- Di Tommaso, D., Stener, M., Fronzoni, G. & Decleva, P. Conformational effects on circular dichroism in the photoelectron angular distribution. *ChemPhysChem* **7**, 924–934 (2006).
- Turchini, S. et al. Conformational effects in photoelectron circular dichroism of alaninol. *ChemPhysChem* **10**, 1839–1846 (2009).
- Tutunnikov, I., Floß, J., Gershnel, E., Brumer, P. & Averbukh, I. S. Laser-induced persistent orientation of chiral molecules. *Phys. Rev. A* **100**, 043406 (2019). Publisher: American Physical Society.
- Tutunnikov, I., Floß, J., Gershnel, E., Brumer, P. & Averbukh, I. S. Laser-induced persistent orientation of chiral molecules. *Phys. Rev. A* **100**, 043406 (2019).
- Tutunnikov, I., Gershnel, E., Gold, S. & Averbukh, I. S. Selective orientation of chiral molecules by laser fields with twisted polarization. *J. Phys. Chem. Lett.* **9**, 1105–1111 (2018). PMID: 29417812.
- Tutunnikov, I. et al. Enantioselective orientation of chiral molecules induced by terahertz pulses with twisted polarization. *Phys. Rev. Res.* **3**, 013249 (2021).
- Spanner, M., Patchkovskii, S., Frumker, E. & Corkum, P. Mechanisms of two-color laser-induced field-free molecular orientation. *Phys. Rev. Lett.* **109**, 113001 (2012).
- Aharonov, Y. & Anandan, J. Phase change during a cyclic quantum evolution. *Phys. Rev. Lett.* **58**, 1593–1596 (1987).
- Resta, R. Geometry and topology in electronic structure theory. *Lecture notes available at <http://www-dft.ts.infn.it/~resta/gtse>* (cit. on pp. 7, 8) (2015).
- Stapelfeldt, H. & Seideman, T. Colloquium: Aligning molecules with strong laser pulses. *Rev. Modern Phys.* **75**, 543 (2003).
- Ayuso, D. et al. Synthetic chiral light for efficient control of chiral light-matter interaction. *Nat. Photonics* **13**, 866–871 (2019).
- Ayuso, D., Ordóñez, A. F. & Smirnova, O. Ultrafast chirality: the road to efficient chiral measurements. *Phys. Chem. Chem. Phys.* **24**, 26962–26991 (2022).
- Samuel, J. & Bhandari, R. General setting for berry's phase. *Phys. Rev. Lett.* **60**, 2339 (1988).
- Beaulieu, S. et al. Photoexcitation circular dichroism in chiral molecules. *Nat. Phys.* **14**, 484–489 (2018).
- Fehre, K. et al. Strong differential photoion circular dichroism in strong-field ionization of chiral molecules. *Phys. Rev. Lett.* **126**, 083201 (2021).

52. Yang, C. N. On the angular distribution in nuclear reactions and coincidence measurements. *Phys. Rev.* **74**, 764–772 (1948).
53. Schwennicke, K. & Joel, Y.-Z. Enantioselective topological frequency conversion. *J. Phys. Chem. Lett.* **13**, 2434–2441 (2022).
54. Suzuki, Y.-I. Communication: Photoionization of degenerate orbitals for randomly oriented molecules: The effect of time-reversal symmetry on recoil-ion momentum angular distributions. *J. Chem. Phys.* **148**, 151101 (2018).
55. Sakurai, J. J. & Commins, E. D. Modern quantum mechanics, revised edition (1995).
56. Ordonez, A. F. & Smirnova, O. Generalized perspective on chiral measurements without magnetic interactions. *Phys. Rev. A* **98**, 063428 (2018).
57. Ordonez, A. F. & Smirnova, O. A geometric approach to decoding molecular structure and dynamics from photoionization of isotropic samples. *Phys. Chem. Chem. Phys.* **24**, 13605–13615 (2022).
58. Nayfeh, A. Introduction to perturbation techniques, John Wiley & Sons. *New York* (1981).

Acknowledgements

We gratefully acknowledge many enlightening discussions with Misha Ivanov and Sir Michael Berry. We thank Dr. Rui Emanuel Ferreira da Silva, Dr. Álvaro Jiménez Galán, Dr. Kiyoshi Ueda for their comments on the manuscript and Dr. Emilio Pisanty for suggesting the acronym MOCD. O.S. is grateful to Ms. Julia Riedel for important discussions. Funded by the European Union (ERC, ULISSES, 101054696). Views and opinions expressed are however those of the author(s) only and do not necessarily reflect those of the European Union or the European Research Council. Neither the European Union nor the granting authority can be held responsible for them. A.F.O acknowledges funding from the European Union's Horizon 2020 research and innovation programme under the Marie Skłodowska-Curie grant agreement No 101029393. D.A. acknowledges funding from Royal Society (URF/R1/201333).

Author contributions

O.S. developed the concept of the work. A.F.O. and O.S. derived all the formulas. D.A. performed molecular photoionization calculations using the code developed by P.D. The draft of the paper was written by A.F.O. and O.S., all the authors contributed to writing the final version of the manuscript.

Funding

Open Access funding enabled and organized by Projekt DEAL.

Competing interests

The authors declare no competing interests.

Additional information

Supplementary information The online version contains supplementary material available at <https://doi.org/10.1038/s42005-023-01358-y>.

Correspondence and requests for materials should be addressed to Olga Smirnova.

Peer review information *Communications Physics* thanks thanks the anonymous reviewers for their contribution to the peer review of this work. A peer review file is available.

Reprints and permission information is available at <http://www.nature.com/reprints>

Publisher's note Springer Nature remains neutral with regard to jurisdictional claims in published maps and institutional affiliations.



Open Access This article is licensed under a Creative Commons Attribution 4.0 International License, which permits use, sharing, adaptation, distribution and reproduction in any medium or format, as long as you give appropriate credit to the original author(s) and the source, provide a link to the Creative Commons license, and indicate if changes were made. The images or other third party material in this article are included in the article's Creative Commons license, unless indicated otherwise in a credit line to the material. If material is not included in the article's Creative Commons license and your intended use is not permitted by statutory regulation or exceeds the permitted use, you will need to obtain permission directly from the copyright holder. To view a copy of this license, visit <http://creativecommons.org/licenses/by/4.0/>.

© The Author(s) 2023